

Search for Excited Quarks in $q\bar{q} \rightarrow \gamma\gamma$ at the LHC

Satyaki Bhattacharya*, Sushil S. Chauhan[†], Brajesh C. Choudhary[‡] and Debajyoti Choudhury[§]

Department of Physics and Astrophysics, University of Delhi, Delhi 11007, India.

If quarks are composite particles, then excited states are expected to play a rôle in the Large Hadron Collider phenomena. Concentrating on virtual effects, and using a large part of the CMS detection criteria, we present here a realistic examination of their effect in diphoton production at the LHC. For various luminosities, we present the 99% confidence limit (CL) achievable in $\Lambda - M_{q^*}$ parameter space where Λ is the compositeness scale and M_{q^*} the mass of the state. For a q^* of mass 0.5 TeV, $\Lambda \leq 1.55$ (2.95) can be excluded at 99% CL with 30 (200)fb⁻¹ integrated luminosity.

PACS numbers: 12.60.Rc, 13.40.-f, 13.85.Qk

I. INTRODUCTION

The replication of fermion families alongwith the mass hierarchies and mixings has led one to speculate about the possibility of quark-lepton compositeness, namely that the Standard Model (SM) fermions are not elementary at all. The fundamental matter constituents in such theories, very often termed *preons*[1], experience an hitherto unknown force on account of an asymptotically free but confining gauge interaction[2], which would become very strong at a characteristic scale Λ , thereby leading to bound states (composites) which are to be identified as quarks and leptons. In most such models[3, 4], quarks and leptons share at least some common constituents.

If this hypothesis were to be true, it is possible, indeed probable, that excited states of fermions exist at a mass scale comparable to the dynamics of the new binding force. In the simplest phenomenological models [5], the excited fermions are assumed to have both spin and isospin 1/2 and to have both their left- and right-handed components in weak isodoublets (*i.e.* they are vector-like). Since these interact with the SM particles, they may be produced at high-energy colliders and would decay back, radiatively, into an ordinary fermion and a gauge boson (photon, W , Z or gluon). Pair production of charged excited fermions could proceed via s -channel (γ and Z) exchanges in e^+e^- collisions, while for excited neutrinos only Z exchange contributes. Although t -channel diagrams are also possible, they generally give a negligible contribution to the overall pair production cross-section on account of the smallness of the cross-couplings [5]. However, this very same interaction between the excited state, its SM counterpart and a gauge boson may be used to singly produce such states (through both s - and t -channel diagrams). The four LEP collaborations have used these (and other) modes to essentially rule out such excitations almost upto the kine-

matically allowed range [6]. At the HERA, on the other hand, both excited leptons and quarks may be produced singly through t -channel diagrams and these processes have been looked at without any positive results [7].

At the Tevatron, one may either pair-produce the excited quarks (primarily through gauge couplings) or produce them singly via quark-gluon fusion, provided the q^*qg coupling strength is significant. A striking signal of the latter would be an enhancement in the dijet production rate with a peak in the invariant-mass distribution. Whereas the DØ collaboration has also excluded the mass region $200 \text{ GeV} < M_{q^*} < 720 \text{ GeV}$ for excited quarks decaying to two jets [8], the CDF collaboration considered a multitude of decay channels, thereby excluding the mass range of $80 \text{ GeV} < M_{q^*} < 570 \text{ GeV}$ [9, 10].

The presence of such particles would change the phenomenology even if they were too heavy to be produced. Since the confining force mediates interactions between the constituents, it stands to reason that these, in turn, would lead to interactions between quarks and leptons that go beyond those existing within the SM. Well below the scale Λ , such interactions would likely be manifested through an effective four fermion contact interaction [11, 12] term that is an invariant under the SM gauge group. The DØ and the CDF experiments at the Tevatron have searched extensively for excited quarks decaying to different final states as predicted by various models, with the negative results translating to lower bounds on compositeness scale Λ . The DØ collaboration has put a lower bound of $\Lambda \geq 2.0 \text{ TeV}$ at 95% CL from an analysis of dijet production [13]. The CDF collaboration has also put a lower limit of $\Lambda \geq 2.81 \text{ GeV}$ at 95% CL studying the $q\bar{q} \rightarrow e\nu$ process[14]. From a phenomenological study of flavor independent contact interaction for the diphoton final state, the lower bound for the LHC has been estimated to be $\Lambda_{\pm} > 2.88$ (3.24) TeV at 95% CL for an integrated luminosity of 100 (200) fb⁻¹ [15].

As can be readily appreciated, the different production modes (and decay channels, wherever applicable) probe different aspects of the effective theory that governs the low energy interactions of these excited states. In this paper, we seek to concentrate on one such property namely

*Email Address: bhattacharya.satyaki@gmail.com

[†]Email Address: sushil@fnal.gov

[‡]Email Address: brajesh@fnal.gov

[§]Email Address: debchou@physics.du.ac.in

the trilinear coupling of the excited quark to its SM counterpart and the photon. To be more precise, rather than seeking to actually produce these excited states, we would like to investigate their rôle in photon pair production at the LHC. Analogous to the process $e^+e^- \rightarrow \gamma\gamma(\gamma)$ used to probe compositeness at LEP, such an exercise would complement the excited quark direct searches for the mass region above the kinematical threshold. Since diphoton production is both a very simple final state and likely to be well-studied at the LHC, it is of interest to see how well can this mode probe compositeness.

The rest of the paper is organized as follows. In the next section, we discuss the effective Lagrangian for the theory under consideration and the new physics contribution to diphoton production. In section III we discuss various SM backgrounds for the signal. In sections IV and V respectively, we describe the event generation and photon candidate reconstruction. Isolation study for photon is discussed in section VI. Confidence limit calculations and results are presented in sections VII and VIII respectively. The systematics is discussed in section IX, and in the last section we summarize this analysis with our conclusions.

II. EXCITED QUARK CONTRIBUTION TO DIPHOTON PRODUCTION

As our interest is not in the production of the excited states, but rather on their contribution to the diphoton rates at a hadronic collider, it suffices to consider only the relevant parts of the Lagrangian, namely the magnetic transition between ordinary and excited states. In general, it is often parametrized by

$$\mathcal{L}_{f^*f} = \frac{1}{2\Lambda} \bar{f}_R^* \sigma^{\mu\nu} \left[\sum_i g_i c_i T_i^a G_{i\mu\nu}^a \right] f_L + h.c., \quad (1)$$

where the index i runs over the three SM gauge groups, viz. $SU(3)$, $SU(2)$ and $U(1)$ and g_i , $G_{i\mu\nu}^a$ and T_i^a are the corresponding gauge couplings, field strength tensors and generators respectively. The dimensionless constants c_i are, *a priori*, unknown and presumably of order unity. Clearly, the phenomenology would depend considerably on the ratios of the constants c_i . For example, electromagnetic couplings (and hence such decays) of such fermions are forbidden if $c_2 = e_f c_1$. Thus, the search strategies would depend crucially on the strengths of these couplings.

A further point needs to be noted here. In the event of any one of the c_i s dominating the others, the cross section for any process governed by the Lagrangian above would scale as some power of the ratio c_i/Λ . Thus, in such a case, it makes sense to eliminate c_i altogether in favour of the unknown scale Λ . Furthermore, with the Lagrangian of eq.(1) being a higher dimensional operator, the cross sections would typically grow with the center of mass energy, consequently violating unitarity. This

is not unexpected in an effective theory as the term in eq.(1) is only the first term and the loss of unitarity, to a given order, is presumably cured once suitable higher dimensional operators are included. An equivalent way to achieve the same goal is to consider the c_i to be form factors rather than constants. To this end, we shall consider the $q^*q\gamma$ vertex to be given by

$$\bar{q}^* q \gamma_\mu(p) \quad : \quad \frac{e}{\Lambda} \left(1 + \frac{Q^2}{\Lambda^2} \right)^{-n} \sigma_{\mu\nu} p^\nu \quad (2)$$

where Q denotes a relevant momentum transfer. It can be checked that, for $Q^2 = s$, unitarity is restored as long as the constant $n \geq 1$. In the rest of our analysis, we shall confine ourselves to a discussion of $n = 1$. While this might seem to be an optimistic choice, it is not quite so. As can be readily appreciated, such a form factor plays a non-negligible rôle only when $Q^2 \gtrsim \Lambda^2$. Since, at the LHC, we shall prove to be sensitive to Λ of the order of a few TeVs, clearly the form factor plays only a marginal rôle in the determination of the sensitivity reach.

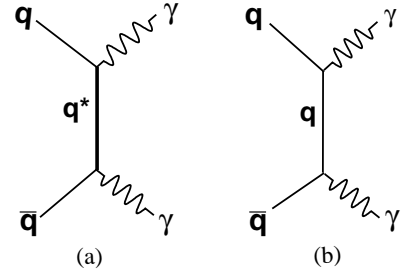


FIG. 1: Production process for diphoton final state (a) Excited quark mediated (b) SM production.

With the introduction of the new (flavour-diagonal) vertex as in eq.(2), the process $q\bar{q} \rightarrow \gamma\gamma$ acquires a new contribution as portrayed in Fig.1. The differential cross section for the partonic process now reads

$$\begin{aligned} \frac{d\sigma}{dt} &= \frac{\pi \alpha^2}{3 \hat{s}^2} \left[e_q^4 \left(\frac{\hat{u}}{\hat{t}} + \frac{\hat{t}}{\hat{u}} \right) - \frac{2e_q^2}{\Omega^2} \left(\frac{\hat{t}^2}{\hat{T}} + \frac{\hat{u}^2}{\hat{U}} \right) \right. \\ &\quad \left. + \frac{1}{\Omega^4} \left\{ \hat{t} \hat{u} \left(\frac{\hat{t}^2}{\hat{T}^2} + \frac{\hat{u}^2}{\hat{U}^2} \right) + M_{q^*}^2 \hat{s} \left(\frac{\hat{t}}{\hat{T}} + \frac{\hat{u}}{\hat{U}} \right)^2 \right\} \right] \\ \Omega &\equiv \Lambda \left(1 + \frac{\hat{s}}{\Lambda^2} \right)^n \\ \hat{T} &\equiv \hat{t} - M_{q^*}^2 \quad \quad \hat{U} \equiv \hat{u} - M_{q^*}^2 \end{aligned} \quad (3)$$

where the SM result is recovered in the limit $\Lambda \rightarrow \infty$. The new physics contribution to the differential cross section thus depends on only two parameters, namely Λ and the mass of the excited state M_{q^*} . For simplicity, we assume these to be flavour-independent (within a generation, it obviously has to be so). For eq.(1) to make sense

as an effective Lagrangian, the masses have to be less than Λ (Ref.[16] requires that $M_{q^*} < \Lambda/\sqrt{2}$).

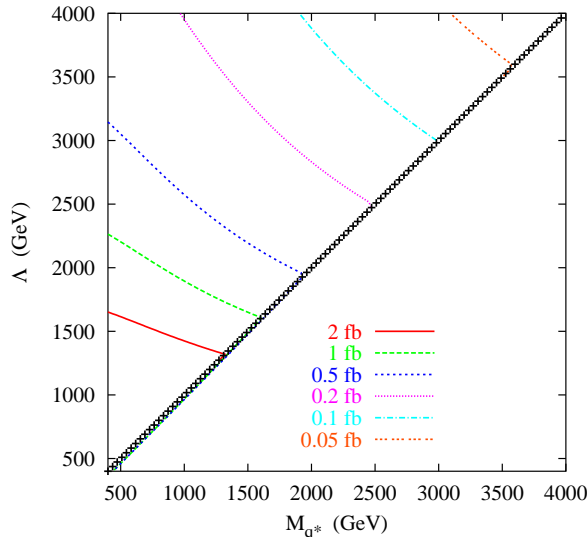


FIG. 2: The contribution of new physics to the total cross section.

In Fig. 2, we present the additional contribution to the total diphoton cross section accruing from the new physics terms in eq.(3). Note that, unlike the QED contribution, this additional contribution does not suffer from collinear singularities.

Contrary to the case of actual production (and subsequent decay) of the excited state, the case under consideration is not associated with any resonant peak. Nevertheless, the presence of the new contribution preferentially enriches the large invariant mass end of the diphoton spectrum. The exchange of a large mass particle in the t - and u -channels naturally enhances the high- p_T photon sample. To improve the signal to noise ratio, we must then concentrate on such a phase-space restricted subset of the final state.

As can be gleaned from a cursory examination of eq.(3), the aforementioned dependence of the new contribution on the photon p_T is not as extreme as that for the QED contribution. Thus, the imposition of such cuts as we will discuss later would not drastically change the shape of the iso-cross section contours as depicted in Fig 2. Consequently, the exclusion contours that we shall finally obtain would bear considerable similarity with those in Fig 2.

III. BACKGROUND

Standard Model processes, understandably, produce a large background to the diphoton final state. The background can be divided into two categories:

- where two prompt photons are produced in the (hard) subprocess itself, and
- in a $\gamma + jet$ sample, a jet with a large electromagnetic fraction (e.g, π^0, ω, η etc.) fakes a photon or a hard photon is produced in the process of fragmentation.

The first category is dominated by the Born-level process $q\bar{q} \rightarrow \gamma\gamma$. An additional source of the diphoton final state is provided by the $gg \rightarrow \gamma\gamma$ process induced by a box diagram. Although the cross-section for this process is relatively small compared to the Born production (in fact, much smaller if very forward photons were to be included) the much larger gg luminosity at the LHC energies implies that $gg \rightarrow \gamma\gamma$ can be quite important. Indeed, even after imposing our selection criteria (to be discussed later) of moderately low rapidities and high transverse momenta for the photons, the gg -initiated contribution is approximately 6.8% of the Born contribution (see Table I).

TABLE I: Various SM cross-sections for $\hat{P}_T \geq 190$ GeV and $|\eta| < 2.7$ at $\sqrt{s} = 14$ TeV. \hat{P}_T , the CKIN(3) parameter in PYTHIA, is the P_T of the outgoing partons in center of momentum frame in a $2 \rightarrow 2$ hard scattering process.

Process	Cross-Section (fb)
$\gamma + jet$	48970
$q\bar{q} \rightarrow \gamma\gamma$ (Born)	76.05
$gg \rightarrow \gamma\gamma$ (Box)	5.18

Apart from the Born and box processes, single photon production processes $qg \rightarrow \gamma q$, $q\bar{q} \rightarrow \gamma g$ and $gg \rightarrow \gamma g$ where a jet fakes a photon can be a major source of background. We have considered all these processes for the background estimation. Although the probability of a jet faking a photon is $\sim 10^{-3} - 10^{-4}$, the cross section for the first two of these hard processes ($qg \rightarrow \gamma q$, $q\bar{q} \rightarrow \gamma g$) are larger by a typical factor of $\mathcal{O}(\alpha_s/\alpha)$ apart from a single ratio of gluon to quark densities, thereby partly recompensing for this suppression. The third process, viz. $gg \rightarrow \gamma g$, is once again box-mediated and significantly smaller than the other two. Similar considerations hold for the background from dijet production with both jets being identified as photons. While the dijet cross section is very large, isolation requirements reduce it drastically. Even a simple estimate, without a full simulation, shows it to be quite unimportant for the physics under investigation.

IV. MONTE CARLO SIMULATION & CUTS

To generate the signal as well as the background events, we have used the PYTHIA [17] event generator wherein the signal matrix element of Eq.(3) had been properly incorporated inside the PYTHIA framework. It

was also counterchecked with a parton-level Monte Carlo generator. We have used the CTEQ5L parton distributions [18], with a choice of $Q^2 = \hat{s}$ for the factorization scale. While generating events, the multi parton interaction (MPI), initial state radiation (ISR) and final state radiation (FSR) switches in PYTHIA were kept “ON”.

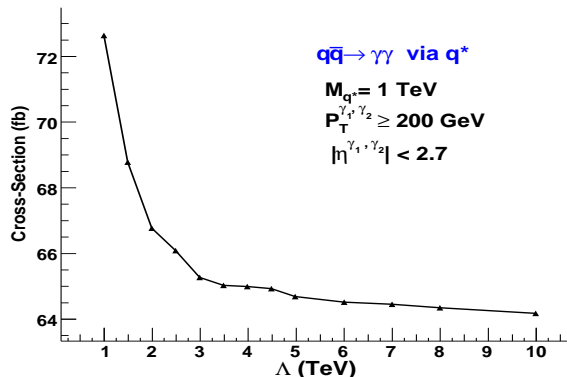


FIG. 3: Variation of cross section with Λ at $\sqrt{s} = 14$ TeV

In view of the fact that the signal events preferentially populate the large transverse momentum part of the phase space, events were generated with $\hat{P}_T \geq 190$ GeV (CKIN(3) parameter) and $|\eta| < 2.7$ respectively. This also rids us of a very large fraction of the SM events which, understandably, are peaked at small angles to the beam-pipe as also small transverse momenta. Fig. 3 shows the variation in cross section with Λ for a fixed value of $M_{q^*} = 1.0$ TeV. Clearly, the variation is well-approximated by a Λ^{-2} contribution superimposed upon a constant (the SM value). This is reflective of the fact that, for large Λ , the new physics contribution is dominated by the interference term in Eq.(3) rather than the pure Λ^{-4} term. Only if we had imposed harder cuts on the photons, would the latter term have dominated (albeit at the cost of reducing event numbers and hence the sensitivity).

It must be noted at this stage that, in the final selection, we have used the fiducial volume of the electromagnetic calorimeter of the CMS detector i.e. $|\eta| < 2.5$ with $1.444 \leq |\eta| \leq 1.566$ excluded on account of the insensitive region between the barrel and the endcaps[19].

V. PHOTON CANDIDATE

Since the SM $\gamma + jet$ and jet-jet production processes form a significant background to $q\bar{q} \rightarrow \gamma\gamma$ via q^* exchange, it is very important to understand the mechanism of a jet faking a photon. The identification of a reconstructed object as a photon candidate depends on the specific design of the detector and the reconstruction algorithm. Taking this into consideration, at the generator level, we have used a clustering algorithm to account for

fake photons arising from jets [20]. The CMS experiment uses $PbWO_4$ crystals for the electromagnetic calorimeter (ECAL). Each crystal measures about $22 \times 22 \text{ mm}^2$ [21] and covers 0.0175×0.0175 (1°) in the $\Delta\eta - \Delta\phi$ space (ϕ being the azimuthal angle). For photon reconstruction, we have used the “hybrid” algorithm [19]. The first step is to find a seed above a certain minimum transverse momentum threshold P_T^{min} of 5 GeV[21]. Only electromagnetic objects, i.e., γ, e^+ and e^- are chosen as seed. Subsequently, one looks for all electromagnetic particles around the seed in the $\eta - \phi$ space where $\Delta\eta$ and $\Delta\phi$ distance from the seed object is at most 0.09. This extension is equivalent to 10×10 crystal size in the CMS detector. The CMS experiment uses 5×5 crystal size to form an energy cluster and nearby non-overlapping clusters are merged to reconstruct a photon candidate. However, in our effort to mimic this reconstruction process at the generator level, we choose to be conservative and use only a 10×10 crystal. We define the momentum of a photon candidate to be the vector sum of the momenta of the electromagnetic objects in such a crystal. A photon candidate will be either a direct photon or other electromagnetic objects such as $\pi^0 \rightarrow \gamma\gamma, \rho^0 \rightarrow \gamma\gamma$ etc. Events where the two highest E_t photons have $\cos(\theta_{\gamma 1 \gamma 2}) > 0.9$ with $\theta_{\gamma 1 \gamma 2}$ being the opening angle between the two photons, are not considered because they could merge into a single energy cluster in the real detector. We have compared our results with the fast detector simulation (FAMOS[22]) used for CMS experiment and they are found to be in good agreement. With this algorithm and requiring the photon to be isolated (to be discussed later), the estimated probability of a jet faking a photon in $\gamma + jet$ channel is $\sim 10^{-3} - 10^{-4}$. The major sources of fake photons are π^0 ($\sim 81\%$), η ($\sim 12\%$) and ω ($\sim 3\%$), with only a small fraction coming from other sources.

VI. ISOLATION VARIABLES

In a detector, a photon is recognised as a local deposition of electromagnetic energy in a limited region in the $\eta - \phi$ phase space. In practice, it is defined as electromagnetic energy contained in a cone of a given size $R \equiv \sqrt{\Delta\phi^2 + \Delta\eta^2}$ with no associated tracks. Fake photon signals arising from a jet can be rejected by requiring either the absence of charged tracks above a certain minimum transverse momentum (P_{Tmin}^{trk}) associated with the photon or the absence of additional energetic particles in an annular cone (R_{iso}) around the photon candidate. We have considered two variables for the isolation purpose (a) the number of tracks (N_{trk}) inside a cone around the photon and (b) the scalar sum of transverse energy (E_{TSUM}) inside a cone around the photon.

A. Track Isolation

We have considered “stable” charged particles e.g. π^\pm , K^\pm , e^\pm and P^\pm as tracks. Of these, π^\pm alone contribute $\sim 80\%$ of the total charged tracks. The contributions from stable charged particles other than the ones mentioned above are negligible. The distributions of the number of charged tracks with a requirement on the transverse momentum of the tracks pointing to either the leading photon or the second leading photon candidate and within a corresponding cone of size 0.35 are shown in Fig. 4. In the signal sample (although we demonstrate for a particular value of the parameters, the features are generic), both photon candidates are true photons and hence the distribution falls very rapidly. The situation is markedly different for the background. For a true $\gamma + jet$ event, the second leading photon is usually the fake one and has a large amount of hadronic activity around it. Consequently, the distribution (in Fig. 4b) reaches a maximum around 5–6 tracks and then falls slowly. To understand the shape of the background distribution in Fig. 4a, it should be realized that a small fraction of such events would actually have the fake photon as the leading one. Since such photons have a large number of tracks around them, an extended tail as seen in Fig. 4a results. The same effect leads to the rise in the background distribution for the second-leading photon for $N_{trk} \leq 1$ (Fig. 4b).

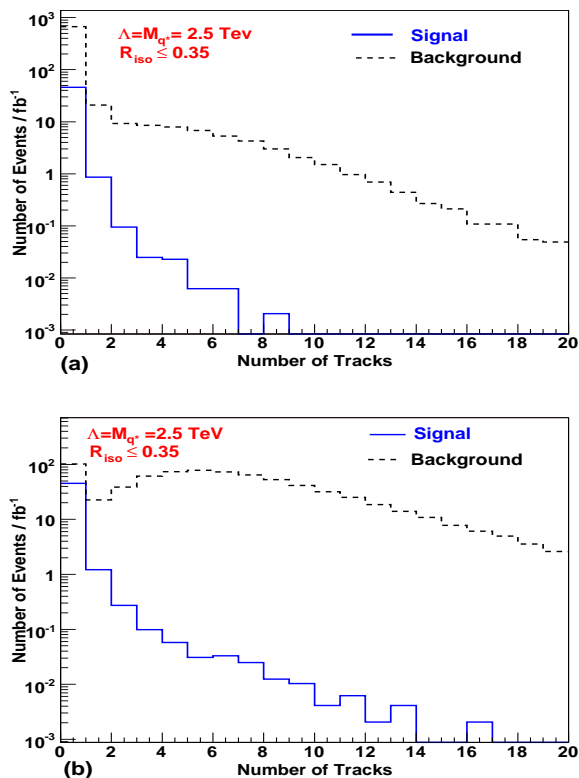


FIG. 4: Number of tracks for the signal and the background events with $P_T^{trk} \geq 3.0$ GeV pointing (a) leading photon and (b) second leading photon candidates in a cone of size 0.35.

In pp collisions at the LHC, one expects to have a large number of soft tracks from associated minimum bias and underlying events. The major sources of tracks in the case of a true photon case are ISR, FSR and MPI, while the low- P_T^{trk} (< 1.5 GeV) tracks emanate mainly from the debris of the colliding protons. If these tracks are counted, a true isolated photon emitted from a hard pp collision may also appear non-isolated, thereby reducing the signal efficiency. To avoid such possibilities, soft tracks are cleaned up by requiring the tracks to have a P_T above a certain minimum threshold (P_{Tmin}^{trk}). In various CMS studies P_{Tmin}^{trk} typically varies between 1-2 GeV [20, 23, 24].

In this analysis, we have considered several choices for P_{Tmin}^{trk} , namely 0.0, 1.0, 2.0 and 3.0 GeV respectively, and for different isolation cone sizes. The signal efficiency and the signal over background (S/B) ratio were calculated with these choices for P_{Tmin}^{trk} and for various N_{trk} possibilities. The results, for the second leading photon, are displayed in Fig. 5. As one can observe, for $N_{trk} = 0$, as P_{Tmin}^{trk} is increased from 1.0 GeV to 3.0 GeV, the signal efficiency increases by more than 15% with only a small reduction in the S/B ratio. Although, allowing more tracks in a given cone size leads to an increase in the signal efficiency, the S/B ratio decreases drastically (see Fig. 4).

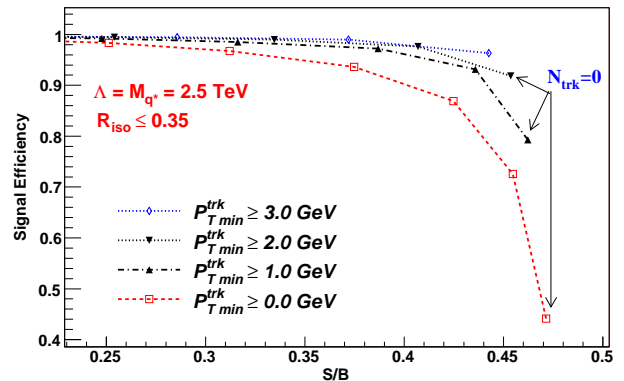


FIG. 5: Effect of the minimum threshold for track P_T on the S/B vs efficiency distribution for the second leading photon.

Understandably, neither the SM diphoton contribution (whether the Born or the box-mediated processes) nor the new physics contribution to the same are affected by the requirement of $N_{trk}=0$. Only the $\gamma + jet$ background suffers. Fig.6 shows the corresponding distribution in P_T for the highest transverse momentum track emanating from the second leading photon. Both the distributions (signal and background) have been normalized to unity. Clearly, the background dominates the signal for $P_{Tmin}^{trk} > 3.5$ GeV, thus pointing out a means to reject a large fraction of the $\gamma + jet$ background. Only those events are accepted where neither of the photons have an associated track with $P_T \geq 3.0$ GeV within the respec-

tive isolation cones (i.e. $N_{trk}=0$ for $P_T^{trk} \geq 3.0$ GeV). Only the highest P_T track is considered because considering lower P_T tracks may affect signal efficiency. Since this study has been done at the generator level we have chosen $P_{Tmin}^{trk} \geq 3.0$ GeV.

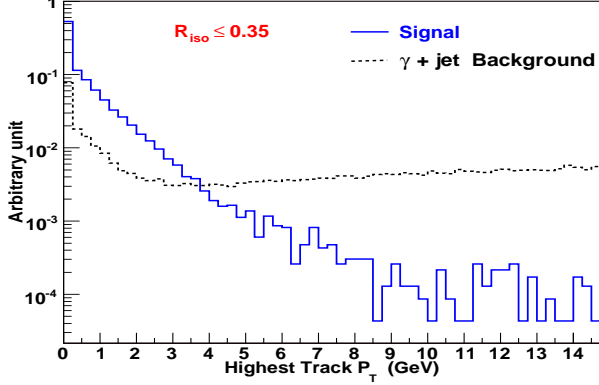


FIG. 6: Highest track P_T around the second leading photon for both signal and $\gamma + jet$ background. An isolation cone of size 0.35 has been used.

B. E_t Sum Isolation

Defined as the cluster of energy inside a cone ΔR from which the energy of the photon is subtracted, the variable E_{TSUM} can be used to discriminate against an event wherein a jet fakes a photon. Although, in a real detector, E_{TSUM} is separately accounted for in the electromagnetic and the hadronic calorimeters, due to limitations of a generator level study, we use a combined E_{TSUM} which is the scalar sum of transverse energy of the electromagnetic and hadronic particles around the photon candidate.

Fig. 7 shows the normalized E_{TSUM} distributions for the signal and the backgrounds. The main aim of this study is to optimize the E_{TSUM} isolation variable so as to reduce the background from $\gamma + jet$ events. The leading photons, expectedly, have similar distribution for the signal and the background. For the second photon though, the behaviours are very different. Most of the $\gamma + jet$ events have $E_{TSUM} > 5$ GeV and by $E_{TSUM} \gtrsim 10$ GeV, the S/B ratio is miniscule.

In Fig. 8, we show the variation in signal efficiency and the S/B ratio for different cone sizes around the second leading photon. Each point corresponds to a different E_{TSUM} threshold, varied in steps of 1 GeV beginning with 1.0 GeV. The final choice of the cone size and the E_{TSUM} threshold depends on the track isolation efficiency, the signal efficiency, and the S/B ratio.

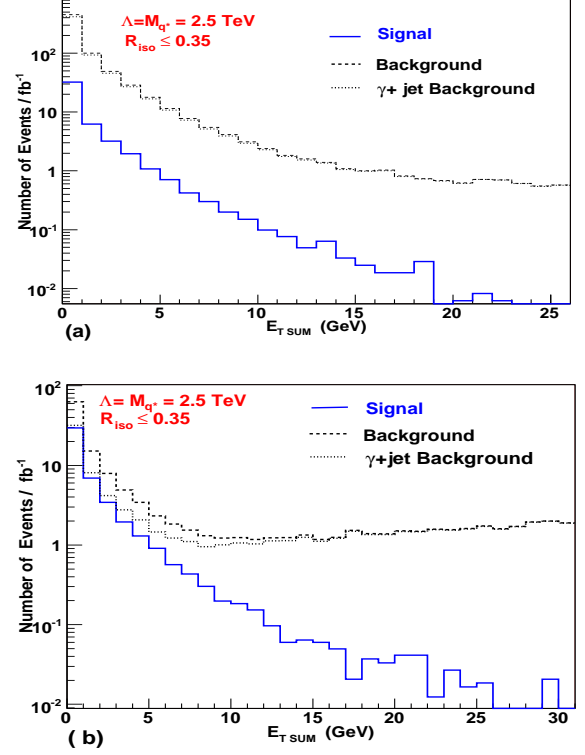


FIG. 7: E_{TSUM} for the signal and the background events around (a) the leading and (b) the next leading photons.

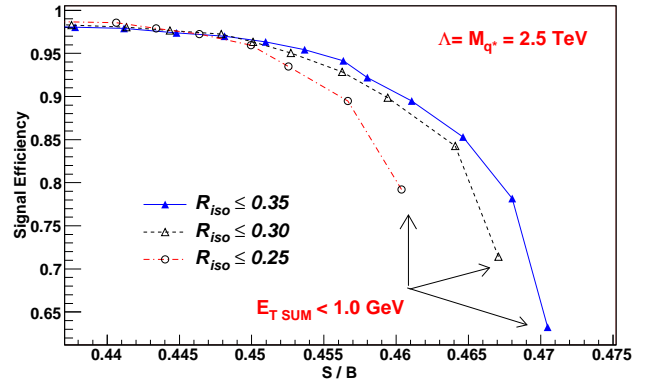


FIG. 8: Signal efficiency vs. S/B ratio for different cone sizes for different choices of the E_{TSUM} threshold around the second leading photon.

C. Combined Isolation

In Table II, we show various combinations of isolation variables for two different cone sizes. Since we aim to observe an excess of diphoton production over the SM expectations, it is rather important to have a large signal efficiency. We have performed this study for a large number of $\Lambda - M_{q*}$ points for which the cross section is

TABLE II: Fraction of events surviving for signal and background after applying isolation cuts on both photons (and the P_T^γ & η^γ criteria). Also shown is the S/B ratio.

R_{iso}	N_{trk}	E_{TSUM}^{max} (GeV)	P_{Tmin}^{trk} (GeV)	S^a (%)	Born (%)	Box (%)	$\gamma + Jet$ (%)	S^a/B
0.35	0	4.0	1.5	75.53	75.45	71.86	0.81	0.828
			2.0	80.52	80.40	76.84	0.90	0.824
			3.0	83.33	83.19	79.57	0.96	0.821
	5.0	5.0	1.5	77.10	77.05	73.60	0.86	0.824
			2.0	83.15	83.05	79.68	0.98	0.818
			3.0	87.18	87.19	83.79	1.09	0.810
	0	4.0	1.5	81.20	80.99	77.97	0.97	0.817
			2.0	85.73	85.59	82.55	1.07	0.811
			3.0	88.49	88.32	85.44	1.15	0.806
0.30	5.0	5.0	1.5	82.25	82.17	79.10	1.01	0.813
			2.0	87.48	87.45	85.45	1.14	0.805
			3.0	91.30	91.24	88.39	1.26	0.798

^aHere $\Lambda = M_{q^*} = 2.5$ TeV

slightly larger than $q\bar{q} \rightarrow \gamma\gamma$ production cross section, or in other words those points for which there will be only a small excess over the SM background. Although we have used a simple approach, it is possible to have other criteria to select analysis points for the choice of final selection cuts. Based on the studies detailed above, the final selection cuts are as follows:

- $P_T^{\gamma 1} \geq 200$ GeV, $P_T^{\gamma 2} \geq 200$ GeV;
- $|\eta^{\gamma 1, \gamma 2}| < 2.5$ & $|\eta^{\gamma 1, \gamma 2}| \notin [1.4442, 1.5666]$;
- $\cos(\theta_{\gamma 1 \gamma 2}) \leq 0.9$;
- $N_{trk} = 0$ for $P_T^{trk} \geq 3.0$ GeV within $R_{iso} \leq 0.35$;
- $E_{TSUM} < 5.0$ GeV within $R_{iso} \leq 0.35$.

After the application of the fiducial volume and photon P_T criteria, the requirement on angular separation between the photons removes only $\sim 1\%$ events.

Table III shows the number of events surviving for signal, Born, box, $\gamma + jet$ and total background for $1fb^{-1}$ of integrated luminosity after applying the final selection criteria.

Fig. 9 shows the distributions for some of the variables for the generated signal and background events after the selection requirements are imposed. In Fig 9f, θ^* is the angle between the direction of boost of the diphoton system and each photon in the diphoton rest frame.

VII. CONFIDENCE LEVEL CALCULATION

As the q^* appears only in the t -channel, no resonance peak appears in the diphoton invariant mass distribution. Rather, a discovery needs to be made from an observation of enhanced rate in the diphoton channel as well as differences in the shape of diverse phase space

TABLE III: The number of events surviving for signal and background for $L_{int} = 1fb^{-1}$ after applying the final selection criteria.

R_{iso}	N_{trk}	E_{TSUM}^{max} (GeV)	P_{Tmin}^{trk} (GeV)	S^a	Born	Box	$\gamma + Jet$	Tot.Back.
0.35	0	4.0	1.5	46.32	35.23	1.90	5.67	42.81
			2.0	49.31	37.54	2.03	6.29	45.87
			3.0	51.09	38.85	2.10	6.70	47.66
	5.0	5.0	1.5	47.33	35.98	1.94	5.99	43.92
			2.0	50.94	38.78	2.11	6.84	47.73
			3.0	53.54	40.71	2.21	7.56	50.49
0.30	0	4.0	1.5	49.83	37.82	2.06	6.74	46.62
			2.0	52.55	39.96	2.18	7.46	49.62
			3.0	54.35	41.24	2.26	8.00	51.51
	5.0	5.0	1.5	50.57	38.35	2.09	7.01	47.46
			2.0	53.67	40.83	2.23	7.93	51.00
			3.0	56.10	42.60	2.34	8.78	53.75

^aHere $\Lambda = 1.0$ TeV and $M_{q^*} = 0.5$ TeV

distributions. In this analysis, we primarily use the information contained in the invariant mass distribution to distinguish between two hypotheses, namely the signal + background hypothesis (S+B) and the background only (B) hypothesis. We adopt a frequentist approach to determine the confidence level of rejecting the S+B hypothesis (the exclusion CL) in the absence of a signal. The histograms shown in Fig.9(e) are used to generate two sets of Gedankenexperiments. To do so, we assume that the content of each bin in the histograms is Poisson distributed. For every bin, we generate a Poisson random number, taking the original bin content as the mean. These Poisson fluctuated random numbers now represent the bin contents of a histogram which we call the outcome of a single Gedankenexperiment. One million such Gedankenexperiments are generated from the S+B histogram (and, similarly, from the B histogram). From each of these experiments we calculated our test statistic, namely

$$\chi_{S+B}^2 = \sum_{i=1}^{n_{bins}} \frac{(d_i - (S+B)_i)^2}{(\sqrt{(S+B)_i})^2} \quad (4)$$

(and similarly for χ_B^2). Here, d_i is the number of events in the i^{th} bin of the $M_{\gamma\gamma}$ distribution as generated in a particular Gedankenexperiment and $(S+B)_i$ is the number of events in the original histogram of $M_{\gamma\gamma}$ obtained from PYTHIA. The distribution of χ^2 shows how the test statistic will be distributed over many repeated observations of the mass histogram. In Fig. 10, the solid histogram shows the expected distribution of χ^2 if the S+B hypothesis is true while the dotted one shows the χ^2 distribution if the S+B hypothesis is not true. The most probable value of χ^2 if S+B is false is given by the peak of the χ_B^2 distribution. The area, α of the χ_{S+B}^2 curve to the right of this value is the probability of seeing a χ^2 value $\geq \chi_B^2$ (peak) if the S+B hypothesis is true. For every point in the (Λ, M_{q^*}) plane satisfying

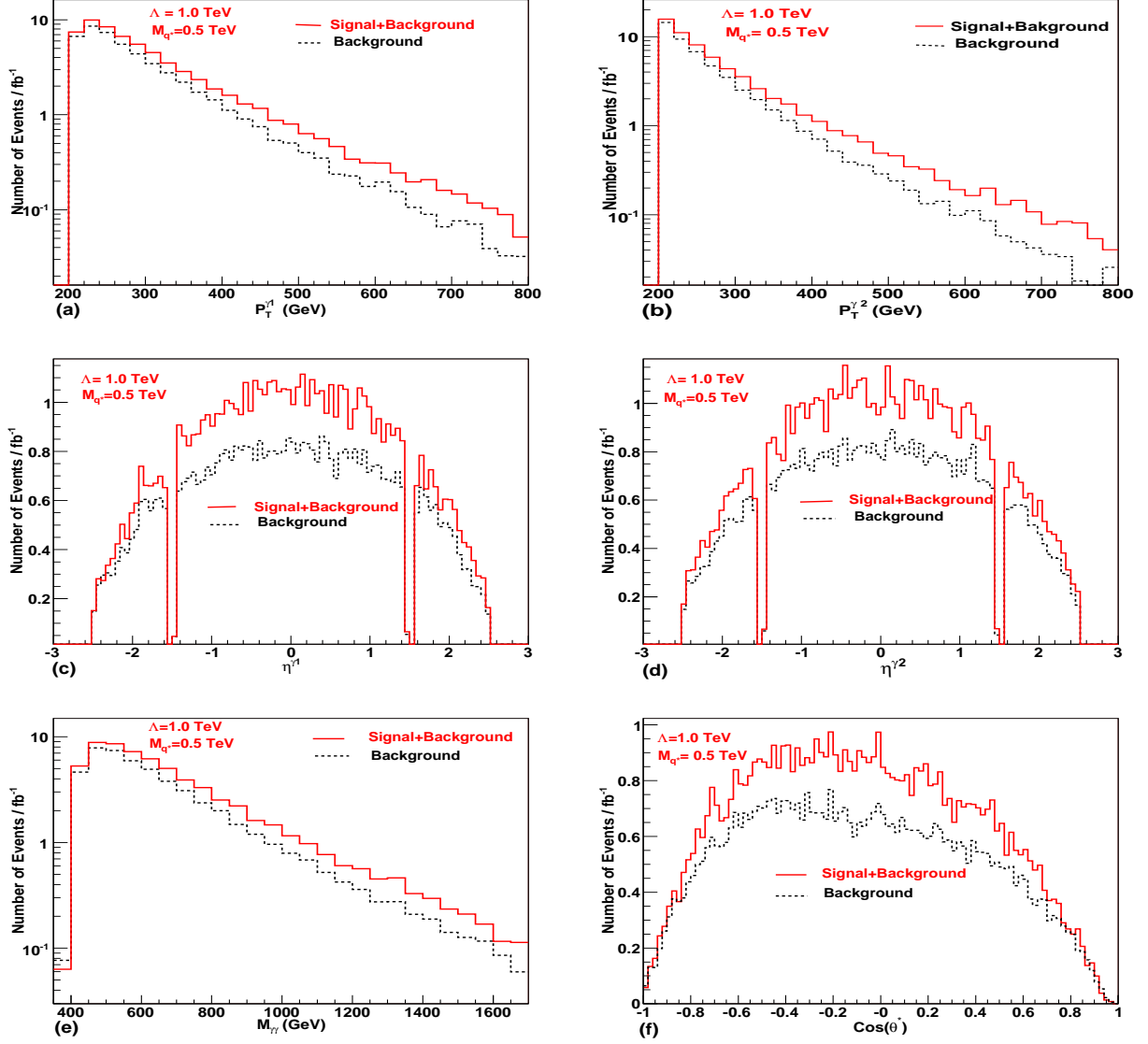


FIG. 9: Kinematic variables after the selection cuts.(a) $P_T^{\gamma 1}$ distribution,(b) $P_T^{\gamma 2}$ distribution,(c) $\eta^{\gamma 1}$ distribution,(d) $\eta^{\gamma 2}$ distribution,(e) $M_{\gamma\gamma}$ distribution and (d) $\cos\theta^*$.

$1 - \alpha \geq 99\%$, the point is rejected at 99% CL.

In calculating the χ^2 , only bins with large significance are used. These have large bin contents and the latter can be safely assumed to be Gaussian distributed. As a consequence, the χ^2 statistic detailed above is equivalent to a log likelihood statistic for this analysis.

Since we have used histograms generated from PYTHIA as our input for the CL extraction there is statistical uncertainty associated with the procedure, i.e., in a repeat of this MC study the position of the χ_B^2 peak will fluctuate, resulting in a different value of α . However at $1 - \alpha = 99\%$, this fluctuation is estimated to be less than 0.5% on either side of the peak.

VIII. RESULTS

Fig. 11 shows the $\Lambda - M_{q^*}$ parameter space which can be excluded for 30, 50, 100 and 200 fb^{-1} of integrated luminosity. To calculate the limits, we have used the invariant mass as the discriminating variable. Since the distribution has a long tail, the analysis has been restricted to $M_{\gamma\gamma} < 1.5$ TeV, so as to have sufficient events for the considered luminosity. The lower limit in the $M_{\gamma\gamma}$ was essentially determined by the requirements on P_T^γ .

We have checked the stability of the limits and found that the 99% CL values suffers only a very small error ($< 0.5\%$) from the uncertainty in the position of the χ_B^2

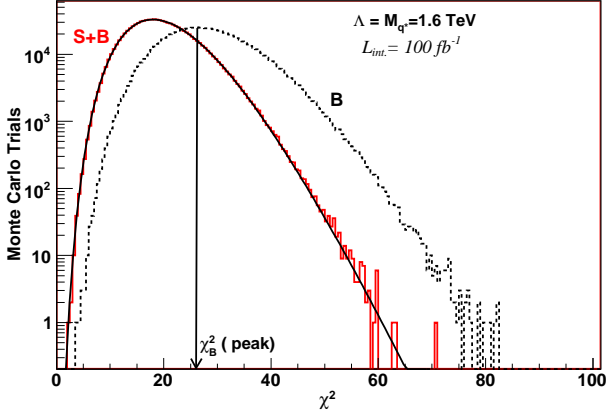


FIG. 10: χ^2 distribution for $S + B$ and B type hypothesis for a given $\Lambda - M_{q^*}$ point with 10^6 MC trials at 100 fb^{-1} of integrated luminosity. Here $S + B$ is fitted with χ^2 distribution.

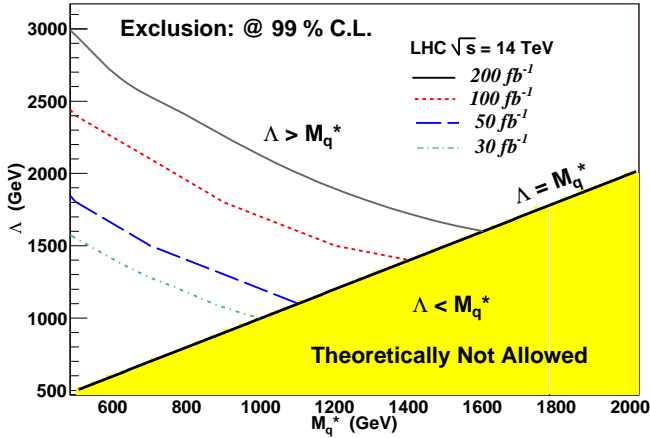


FIG. 11: Achievable exclusion contours in the $\Lambda - M_{q^*}$ parameter space corresponding to different integrated luminosities at the LHC. The regions below the curves can be ruled out at 99% C.L.

peak as determined from Monte Carlo trials. To find the dependence on the choice of kinematical cuts, we reduced the fiducial volume from $|\eta| < 2.5$ to $|\eta| < 1.5$. This changes the CL from 98% to 99% CL. Similarly the 98% CL limits obtained with $P_T^\gamma \geq 200 \text{ GeV}$ changes to 99% CL at $P_T^\gamma \geq 250 \text{ GeV}$ but at the cost of severe loss in signal efficiency. Since we have used the deviation of the invariant mass from the SM prediction as a discriminating variable, we expect to further improve the limit by combining some other uncorrelated variables[26].

IX. SYSTEMATICS

As described in the earlier sections, we have performed a detailed analysis including a realistic simulation of the various detector effects and uncertainties. Some systematic uncertainties persist still and, in this section, we present an estimation for each of these.

- **Choice of PDF:** To estimate the uncertainty due to the choice of the PDF, the cross sections were calculated with different choices of PDFs and the results obtained compared with those obtained for CTEQ6M [27]. For comparison we used CTEQ5M1, CTEQ5L and MRST2001. A maximum uncertainty of $\sim 7\%$ was found when CTEQ5L was compared to CTEQ6M. For CTEQ5M1 and MRST2001 these values are 2.3% and 3.5% respectively.
- **Scale Variation:** To estimate this, the factorization scale Q (chosen to be \sqrt{s} in our analysis) was varied from in the range $Q^2 \in [\hat{s}/2, 2\hat{s}]$. Also used was $Q^2 = P_T^2$. In all these variations, the maximum uncertainty was found to be 1.6%.
- **Higher-order effects:** The SM processes relevant to us have been studied in the literature at great length. Most higher order effects can be adequately parametrized in the form of a K -factor. For true diphoton production, these are 1.5 (Born process)[29] and 1.2 (box) [30]. For the $\gamma + jet$ events, these are 1.66 when the quark fragments into a photon [30] and 1.0 when an (almost) isolated π^0 in the hadronic jet fakes a photon [30]. For the new physics contribution, the K -factor is not known though (indeed, the very definition could be ambiguous for a nonrenormalizable theory), and hence we have not used any in our analysis. However, in the limit of a very large M_{q^*} , the new physics effect should be describable in terms of an effective operator involving quarks and photons and the K -factor, in this limit, is not expected to be too different from the SM one [12].
- **Energy resolution:** To study the effect of the detector energy resolution on this analysis, the energy of the photons was smeared with the stochastic term of the CMS electromagnetic calorimeter energy resolution[21]. The effect was found to be negligible.

- Dijet background: Due to limitations in computing resources, we did not fully simulate the background from jet-jet events. Although the dijet cross sections are very large, given the low probability of a jet faking a photon (as described earlier in the text), it is obviously not very likely that too many such events would survive the selection criteria that we have imposed. A parton-level Monte Carlo calculation readily verified this.

Even in the corresponding PYTHIA study, it was again observed that the kinematical and isolation cuts reduces this background drastically. In a sample of 9000 jet-jet events, no event survives the final selection requirements. However, with the same survival efficiency as for $\gamma + jet$ events (i.e., $\sim 1\%$) and with same kinematical and isolation cuts, we expect to have a jet-jet background of less than 3.7 events for an integrated luminosity of $1 fb^{-1}$. Hence we may safely assume that two photon events from jet-jet background will have negligible effect on the final confidence level calculation.

- Luminosity error: At the LHC, for an integrated luminosity above $30 fb^{-1}$, the error on the measured luminosity is expected to be 3% [28].

We have determined the effect of uncertainty in the theoretical cross-section on the CL. To get a conservative estimate we lowered the cross section by 1% and found that 99% CL changes to 98% CL.

X. CONCLUSIONS

To summarise, we have investigated the potential of using the diphoton final state at the LHC in probing possible substructure of quarks. In any model of quark compositeness, excited states occur naturally and these couple to the SM counterparts through a generalised magnetic transition term in an effective Lagrangian. Consequently, the presence of such states would alter the diphoton cross section, the extent of which depends on both the mass M_{q^*} and the compositeness scale Λ . The deviation

concentrates in the large p_T regime, especially for larger M_{q^*} and can be substantial. For example, $\Lambda = M_{q^*} = 1$ TeV leads to a $\sim 12\%$ deviation in the cross section (when restricted to an appropriate part of the phase space as defined in Section IV).

Using the photon reconstruction algorithm as used for the CMS detector at the LHC, we perform a realistic estimation of the deviation caused by the excited quark exchange contribution to the diphoton rate. We have accounted for all major backgrounds to evaluate the limits in the $\Lambda - M_{q^*}$ parameter space. The possible exclusion limits are very strong and depend only weakly on the choice of the kinematical cuts.

While direct searches can lead to very strong limits from the non-observation of mass peaks, the search strategy outlined here can prove to be a complementary tool. In particular, as shown above, this mode is sensitive to excited quark masses far above the kinematical limit for pair-production (which mainly proceeds through gauge interaction). Furthermore, this method is sensitive to the magnetic transition coupling ($q^* q \gamma$) in an unambiguous manner free from all other couplings and parameters of this essentially complex theory.

Acknowledgments

SB and SSC would like to thank Marco Pieri for his comments on photon algorithm whereas DC would like to thank Samir Ferrag for illuminating discussions. SB and DC acknowledge support from the Department of Science and Technology (DST), Government of India under project number SR/S2/RFHEP-05/2006. BCC acknowledge support from the DST, Government of India under project number SP/S2/K-25/96-V. BCC, SB and SSC gratefully acknowledge the facilities provided by the Center for Detector and Related Software Technology (CDRST), University of Delhi. SSC would like to express gratitude to the Council of Scientific and Industrial Research (CSIR), India for financial assistance and to Prof. R.K. Shivpuri and Prof. Raghuvir Singh for support and encouragement.

[1] H. Harari and N. Seiberg, Phys.Lett. **B98** (1981) 269; M.E. Peskin, in *proceedings of the 1981 International Symposium on Lepton and Photon Interaction at High Energy*, W.Pfeil, ed., p880 (Bonn, 1981); L. Lyons, Oxford University Publication 52/82 (June 1982).
[2] G. 't Hooft, in *Recent Developments in Gauge Theories*, G. 't Hooft *et al.*, eds. (Plenum Press, New York, 1980).
[3] J.C. Pati, A. Salam and J.A. Strathdee Phys.Lett. **B59** (1975) 265; H. Fritzsch and G. Mandelbaum, Phys.Lett. **B102** (1981) 319; W. Buchmuller, R.D. Peccei and T. Yanagida, Phys.Lett.

B124 (1983) 67; Nucl.Phys. **B227** (1983) 503; Nucl.Phys. **B237** (1984) 53; U. Baur and H. Fritzsch, Phys.Lett. **B134** (1984) 105; X. Li and R.E. Marshak, Nucl.Phys. **B268** (1986) 383; I. Bars, J.F. Gunion and M. Kwan, Nucl.Phys. **B269** (1986) 421; G. Domokos and S. Kovesi-Domokos, Phys.Lett. **B266** (1991) 87; J.L. Rosner and D.E. Soper, Phys.Rev. **D45** (1992) 3206; M.A. Luty and R.N. Mohapatra, Phys.Lett. **B396** (1997) 161 [hep-ph/9611343]; K. Hagiwara, K. Hikasa and M. Tanabashi,

- Phys.Rev.**D66** (2002) 010001; Phys.Lett.**B592** (2004) 1.
- [4] For a review and additional references, see R.R. Volkas and G.C. Joshi, Phys. Rep. **159** (1988) 303.
- [5] K. Hagiwara, S. Komamiya and D. Zeppenfeld, Z. Phys. **C29** (1985) 115;
U. Baur, M. Spira, and P.M. Zerwas, *Phys. Rev. D* **42** (1990) 815;
F. Boudjema, A. Djouadi and J.L. Kneur, Z. Phys. **C57** (1993) 425.
- [6] ALEPH Collaboration, Phys. Lett. **B385** (1996) 445; *ibid* **B384** (1996) 439; *ibid* **B250** (1990) 172; *ibid* **B236** (1990) 501; *ibid* **B236** (1990) 511;
DELPHI Collaboration, Phys. Lett. **B393** (1997) 245; Zeit. Phys. **C 74** (1997) 57; *ibid* **C 74** (1997) 577; *ibid* **C53** (1992) 41; Phys. Lett. **B274** (1992) 230; *ibid* **B380** (1996) 480; Eur. Phys. J. C **8**, 41 (1999);
L3 Collaboration, Phys. Lett. **B412** (1997) 189; *ibid* **B401** (1997) 139; *ibid* **B377** (1996) 304; *ibid* **B370** (1996) 211; *ibid* **B295** (1992) 371; *ibid* **B251** (1990) 321; *ibid* **B247** (1990) 177; *ibid* **B250** (1990) 205; *ibid* **B252** (1990) 525; *ibid* **B502** (2001) 37;
OPAL Collaboration, Eur. Phys. J. **C1** (1998) 45; Phys. Lett. **B393** (1997) 217; *ibid* **B391** (1997) 197; *ibid* **B386** (1996) 463; *ibid* **B385** (1996) 433; Z.Phys. **C52** (1991) 175; Phys. Lett.**B257** (1991) 531; *ibid* **B247** (1990) 448; *ibid* **B244** (1990) 135; *ibid* **B240** (1990) 250.
- [7] H1 Collab., I. Abt *et al.*, Nucl. Phys. **B396** (1993) 3;
H1 Collab., C. Adloff *et al.*, *Phys. Lett. B* 525 (2002) 9;
H1 Collab., C. Adloff *et al.*, *Phys. Lett. B* 548 (2002) 35;
H1 Collab. C. Adloff *et al.*, *Eur. Phys. J.C* 17 (2000) 567;
ZEUS Collab., M. Derrick *et al.*, Z. Phys. **C65** (1994) 627;
ZEUS Collab., S. Chekanov *et al.*, Phys. Lett. **B 549**, 32 (2002).
- [8] DØ Collaboration, I.A. Bertram, Report No. Fermilab-Conf-96/389-E, (1996).
- [9] CDF Collaboration, F.Abe *et al.*, Phys Rev. Lett. 72, 3004(1994).
- [10] CDF Collaboration, F.Abe *et al.*, Phys Rev. **D74**, 3538(1995).
- [11] R. Rückl, Phys. Lett. **B129** (1983) 363; Nucl. Phys. **B234** (1984) 91;
W. Buchmuller, R. Rückl and D. Wyler, Phys. Lett. **B191** (1987) 442;
P. Haberl, F. Schrempp and H. U. Martyn, in *Physics at HERA*, eds. W. Buchmuller and G. Ingelman, DESY (1991) P.1133;
W. Buchmuller and D. Wyler, Phys. Lett. **B407** (1997) 147 [hep-ph/970431];
N.G.Deshpande, B. Dutta and X.-G. He, Phys. Lett. **B408** (1997) 288 [hep-ph/9705236].
- [12] D. Choudhury, S. Majhi and V. Ravindran, JHEP **0601**, 027 (2006) [hep-ph/0509057];
S. Majhi, arXiv: 0705.3071 [hep-ph].
- [13] B. Abbott *et. el.*, Phy. Rev. **D62**, 031101(2000).
- [14] T. Affolder *et. el.*, Phy. Rev. Lett. 87, 231803(2001).
- [15] T.G. Rizzo, Phy. Rev.**D51**, 1064 (1995).
- [16] P. Hasenfratz and J. Nager, Z. Phys. C **37** (1988) 477.
- [17] T. Sjostrand *et al.*, Comput. Phys. Commun. 135 (2001)238.
- [18] H. L. Lai *et al.* [CTEQ Collaboration], Eur. Phys. J. **C 12**, 375 (2000) [arXiv:hep-ph/9903282].
- [19] CMS Collaboration, "CMS Physics Technical Design Report volume -I", **CERN/LHCC 2006-001** (2006).
- [20] M. Pieri *et al.*, CMS **Note-2006/112**.
- [21] The Electromagnetic Calorimeter Project, Technical Design Report, **CERN/LHCC 97-33**, 15 December 1997.
- [22] FAMOS, "Fast Monte Carlo Simulation", <http://cmsdoc.cern.ch/cms00/projects/FAMOS>.
- [23] P. Gupta *et al.*, CMS **Note-2007/004**; arXiv:0705.2740 [hep-ex].
- [24] L. Fano (On behalf of CMS collaboration), CMS Conference Report -2006/083.
- [25] P.K. Sinervo, CDF/PUB/STATISTICS/PUBLIC/6031, 2002.
- [26] G. Abbiendi *et al.* [OPAL Collaboration], Eur. Phys. J.C **26** (2003) 479.
- [27] J. Pumplin, D. R. Stump, J. Huston, H. L. Lai, P. Nadolsky and W. K. Tung, JHEP **0207** (2002) 012 [arXiv:hep-ph/0201195].
- [28] S. Abduin *et. al.* CMS **NOTE-2006/122**.
- [29] T. Binoth *et al.*, QCD/SM Working Group, Les Houches, 2001.
- [30] Z. Bern, L. Dixon, C. Schmidt, Phys. Rev. **D 66**(2002) 074018.